Progress in Natural Science: Materials International 26 (2016) 289–294

HOSTED BY

Contents lists available at ScienceDirect

Progress in Natural Science: Materials International

journal homepage: www.elsevier.com/locate/pnsmi

Original Research

Atomic layer deposition on Pd nanocrystals for forming Pd-TiO_2 interface toward enhanced CO oxidation

Yu Bai [1], Chunlei Wang [1], Xingyi Zhou, Junling Lu *, Yujie Xiong *

Hefei National Laboratory for Physical Sciences at the Microscale, iChEM (Collaborative Innovation Center of Chemistry for Energy Materials), Hefei Science Center (CAS), and School of Chemistry and Materials Science, University of Science and Technology of China, Hefei, Anhui 230026, China

ARTICLE INFO

Article history:
Received 30 March 2016
Accepted 20 April 2016
Available online 30 May 2016

Keywords:
Pd
Atomic layer deposition
CO oxidation
TiO_2
Charge density

ABSTRACT

Pd typically exhibits relatively low catalytic activity in CO oxidation, as CO is apt to be adsorbed on Pd to poison the surface for O_2 activation. In this Letter, we report that this limitation can be overcome by integrating Pd with TiO_2. The TiO_2 was coated on Pd nanocubes with a controllable thickness using atomic layer deposition (ALD) method. Given the different work functions of TiO_2 and Pd, the electrons in TiO_2 semiconductor will flow toward Pd. With the electron density increased on Pd, the adsorption of CO to Pd will be weakened while the oxygen activation can be facilitated. Meanwhile, the interface-confined sites at Pd-TiO_2 may further enhance the oxygen activation. As the species adsorption and activation are strongly correlated with electron density, the performance of Pd-TiO_2 in CO oxidation turns out to depend on the TiO_2 thickness, which determines the number of transferred electrons, within a certain range (< 1.8 nm). This work provides a new strategy for enhancing catalytic performance through tailoring charge densities in hybrid catalysts.

1. Introduction

Heterogeneous catalysis represents an important route to facilitate various reactions such as CO oxidation, in which reaction species have to be adsorbed and activated on the catalyst surface. Thus the surface charge state of catalysts, which determines the adsorption and activation of reaction species, plays an important role in catalytic reactions [1–3]. For this reason, tuning the surface charge densities would become a versatile tool to improve catalytic performance. In terms of CO oxidation, it generally takes place through three key steps: the adsorption of CO molecules, the dissociative adsorption of O_2, and the formation and desorption of CO_2 [4]. Among these steps, the dissociative adsorption of O_2 is the rate-determining step, whose low efficiency often limits the overall performance of CO oxidation [5].

Pd is a highly active catalytic material for most reactions. In the case of CO oxidation, however, CO is apt to be adsorbed on Pd to poison the surface. This metal poisoning greatly hampers the activation of molecular oxygen at the catalyst surface [6,7]. Given this limitation, we aim to utilize CO oxidation and Pd catalyst as a model system to investigate whether the catalytic performance can be enhanced by tuning surface charge densities. The surface charge density of a material can be maneuvered by forming heterogeneous junctions [1,8,9]. As two materials with different work functions form a junction, a charge transfer process will occur so as to equilibrate the electron Fermi distribution at their junction interface. It provides an opportunity to regulate the surface charge state of materials. For instance, TiO_2 is a widely used semiconductor with a smaller work function than Pd [10], and does not possess catalytic activity for CO oxidation in the dark. When Pd is in intimate contact with TiO_2, electrons will flow from the higher Fermi level of TiO_2 to Pd. This process accumulates negative charges on the Pd and elevates the energy level of electrons. We anticipate that in such a Pd-TiO_2 system, the CO adsorption and O_2 activation can be maneuvered through tunable surface charge states.

In order to establish the relationship between surface charge density and CO oxidation performance, we decide to use an ultrathin-film configuration for TiO_2 integration. The ultrathin-film materials have been widely used for catalytic studies in recent years, owing to their tunable electronic structures [11–14]. In the form of ultrathin films, we can control the number of electrons which transfer from TiO_2 to Pd by tailoring the film thickness. However, it remains a grand challenge to grow TiO_2 ultrathin films on Pd in solution phase.

In this Letter, we report the coating of TiO_2 on cubic Pd nanocrystals (i.e., nanocubes) by employing the ALD technique, an undoubtedly effective method for fabricating ultrathin-film structures [15,16]. Enabled by the ALD technique, the thickness of

* Corresponding authors.
E-mail addresses: junling@ustc.edu.cn (J. Lu), yjxiong@ustc.edu.cn (Y. Xiong).
[1] These authors equally contributed to this work.
Peer review under responsibility of Chinese Materials Research Society.

http://dx.doi.org/10.1016/j.pnsc.2016.05.010

TiO_2 film can be precisely controlled by altering ALD cycles [17]. In addition, the TiO_2 prepared via the ALD technique is amorphous and porous, allowing the reactants CO and O_2 to penetrate the TiO_2 film as well as reach the Pd surface [18,19]. In terms of Pd substrate, the cubic nanocrystals are selected as the substrate geometry due to three reasons: (1) the synthetic system for Pd nanocubes is relatively simple and clean, which facilitates the subsequent deposition of TiO_2 ultrathin films [20]; (2) the well-defined crystal planes ensure that each metal nanocrystal possesses the same surface charge state, which can set up a reliable standard for mechanism studies [21–23]; (3) the flat surface of nanocrystals enables the formation of high-quality interface between Pd and TiO_2, allowing high-efficiency interfacial charge transfer [8,24]. Based on this platform, we reveal that the integration with amorphous TiO_2 ultrathin films can dramatically enhance the catalytic performance of Pd nanocubes in CO oxidation. The performance enhancement indeed has a strong correlation with the thickness of TiO_2 ultrathin films deposited on Pd nanocubes.

2. Experimental details

2.1. Chemicals

Poly(vinyl pyrrolidone) (PVP, M.W.=55,000) was purchased from Aldrich, and K_2PdCl_4 and 3-aminopropyltriethoxysilane (APTES) were purchased from Aladdin. All other chemicals were of analytical grade and purchased from Sinopharm Chemical Reagent Co. Ltd., Shanghai, China. All chemicals were used as received without further purification.

2.2. Synthesis of SiO_2 nanospheres

Typically, 3.6 mL of TEOS and 12 mL of ammonia aqueous solution were added into 88 mL of ethanol in a 500-mL flask. After the mixture was stirred for 5 h at room temperature, 60 μL of ATPES was added to the mixture. Then the reaction was allowed to proceed for 12 h. The product was collected by centrifugation and washed with water three times to remove excess ethanol and ammonia. The obtained powder was dried at 60 °C in a vacuum.

2.3. Synthesis of SiO_2-Pd hybrid structures

7.5 mL of an aqueous solution containing 0.105 g of PVP, 0.06 g of ascorbic acid (AA) and a certain amount of KBr in a 50-mL flask were heated at 80 °C for 10 min under magnetic stirring. Then 0.5 mL of aqueous suspension containing 50 mg of SiO_2 nanosphere was added in using a pipette. Subsequently, 3 mL aqueous solution containing 0.065 g K_2PdCl_4 was added into the flask. The reaction was allowed to continue at 80 °C for 3 h. The product was collected by centrifugation and washed three times with ethanol.

2.4. Synthesis of P25-Pd hybrid structures

The synthesis was performed via a similar procedure to that used for the SiO_2-Pd samples, except that the SiO_2 was replaced with P25 (commercial TiO_2).

2.5. Fabrication of SiO_2-Pd@TiO_2 hybrid structures

The ALD coating of TiO_2 on SiO_2-Pd catalysts was performed in a viscous flow reactor (GEMSTAR-6™ Benchtop ALD, Arradiance) at 120 °C by alternatively exposing titanium isopropoxide (TTIP, 99.7%, Sigma-Aldrich) and Millipore water for different ALD cycles. The TTIP precursor was heated to 80 °C to obtain a reasonable vapor pressure, while the water source was kept at room temperature. The timing sequence of TiO_2 ALD was 8, 200, 5, and 250 s for TTIP exposure, N_2 purge, water exposure and N_2 purge, respectively. The resulted catalysts are denoted as SiO_2-Pd@(n)cycTiO_2 (n: the number of ALD cycles).

2.6. Characterizations

Prior to electron microscopy characterizations, a drop of the aqueous suspension of particles was placed on a piece of carbon-coated copper grid and dried under ambient conditions. Transmission electron microscopy (TEM), high-resolution TEM (HRTEM), scanning TEM (STEM) images and energy-dispersive spectroscopy (EDS) mapping profiles were taken on a JEOL JEM-2100F field-emission high-resolution transmission electron microscope operated at 200 kV. X-ray photoelectron spectra (XPS) were collected on an ESCALab 250 X-ray photoelectron spectrometer, using nonmonochromatized Al-Kα X-ray as the excitation source. The expected charging of samples was corrected by setting the C 1s binding energy of the adventitious carbon to 284.5 eV.

2.7. Catalytic CO oxidation measurements

The activities of SiO_2-Pd catalysts in CO oxidation were evaluated using a fixed-bed tubular quartz reactor at atmospheric pressure in the dark. 30 mg of catalyst, well mixed with 1 g of fine quartz particles (60/80 mesh), was used for the reaction test. For other SiO_2-Pd@(n)cycTiO_2 catalysts, the amount of catalyst was adjusted to keep the same Pd content. Prior to the reaction, the catalyst was first calcined in 10% O_2 in He with a flow rate of 40 mL/min at 150 °C for 60 min. Next, the reaction gas consisting of 1% CO and 20% O_2 balanced with He was fed to the reactor at a total flow rate of 20 mL/min. The reaction products were analyzed by an online gas chromatograph (Fuli, GC-9790II) with a thermal conductivity detector. The CO conversion was calculated based on the ratio of the consumed CO to the fed CO.

3. Results and discussion

As illustrated in Fig. 1a, our hybrid structures between Pd nanocubes and TiO_2 ultrathin films are fabricated through a three-step process. The key to this process is to keep the Pd nanocubes monodispersed so that the TiO_2 can be uniformly coated on each Pd nanocube. In order to prevent the aggregation of Pd nanocubes, we first synthesize the SiO_2 nanospheres with an average diameter of 300 nm which can serve as supports for the entire catalytic nanostructures using an ALD method (Fig. S1a) [25]. It is worth noting that the SiO_2 cannot catalyze CO oxidation (Fig. S1b), so it can serve as an inert support.

In the next step, Pd nanocubes are evenly deposited on the surface of SiO_2 nanosphere by an in-situ growth method, forming the SiO_2-Pd hybrid nanostructures. From TEM and HRTEM images (Fig. S2a), one can see that the produced Pd nanocrystals take a cubic geometry and have an edge length of ca. 10 nm. The single-crystal Pd nanocubes are uniformly distributed on the surface of SiO_2 nanospheres. Fig. S2b shows the Pd 3d XPS spectra of the SiO_2-Pd sample. The Pd $3d_{5/2}$ and Pd $3d_{3/2}$ peaks for the sample are located at the binding energies of 335.0 and 340.3 eV, respectively, confirming that the Pd nanocubes deposited on SiO_2 are in the form of zero valence [26].

Finally, we coat TiO_2 ultrathin films on the Pd nanocubes using TiO_2 ALD to form SiO_2-Pd@TiO_2 nanostructures. As revealed by Fig. 1b and c, the Pd nanocrystals largely maintain their cubic shape after 30 ALD cycles, and are interfaced with TiO_2 ultrathin film with a thickness of about 2.4 nm (namely, SiO_2-Pd@30cyc-TiO_2). Given the low thickness of TiO_2 shells, they

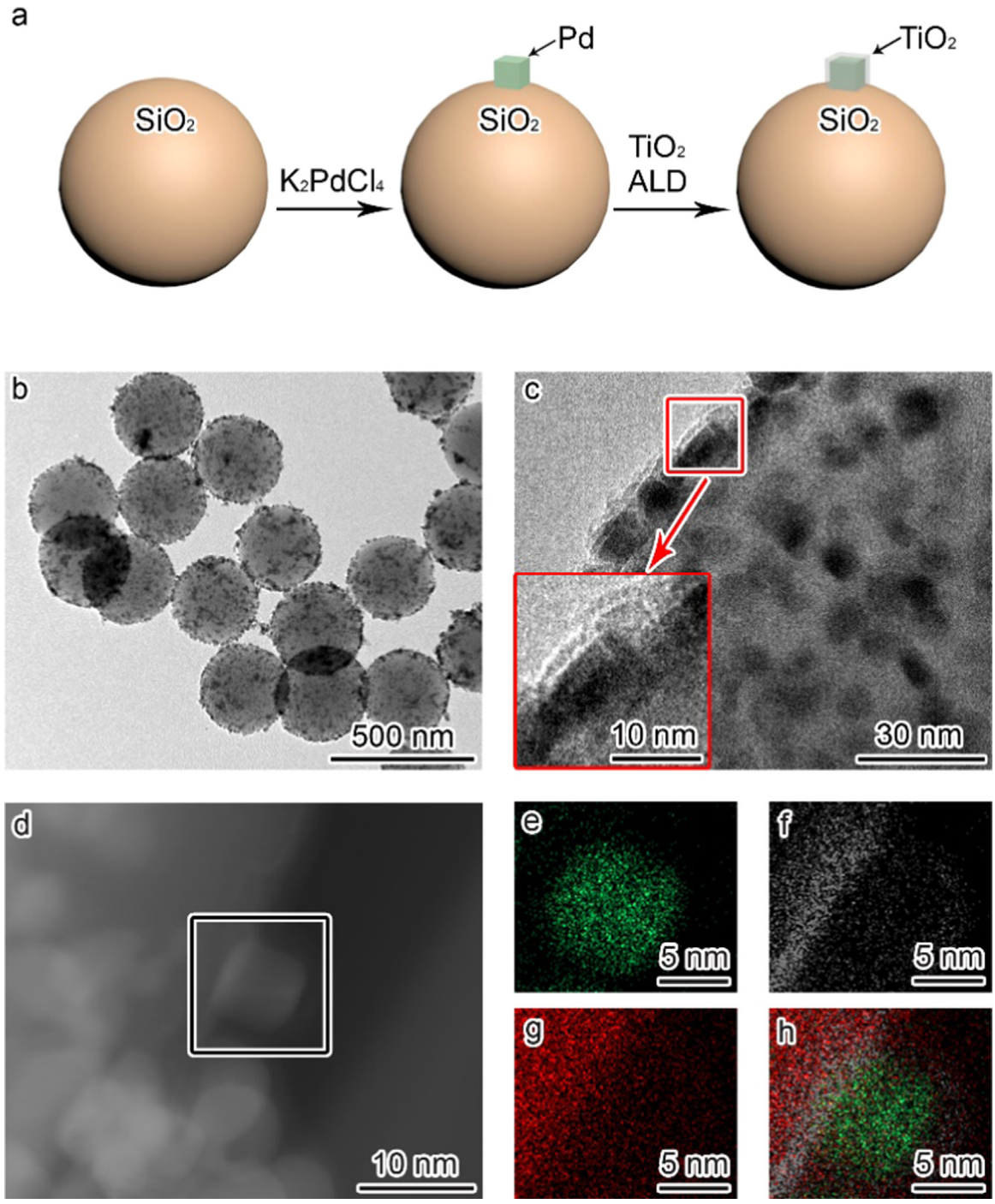

Fig. 1. (a) Schematic illustration for the fabrication of SiO_2-Pd@TiO_2 hybrid structures. (b, c) TEM images of the SiO_2-Pd@TiO_2 structures (namely, SiO_2-Pd@30cyc-TiO_2). The inset of panel c shows a magnified TEM image taken from the corresponding region. (d) STEM image of the Pd@TiO_2 structures supported on SiO_2. (e-h) EDS mapping profiles taken from the region marked by the box in panel d: element profiles for Pd (green) (e), Ti (gray) (f), O (red) (g), and merge (h).

appear to be porous so that small reactant molecules may penetrate through and access the Pd inside in CO oxidation application.

Fig. S3 shows the Ti 2p and Pd 3d XPS spectra of SiO_2-Pd@30cyc-TiO_2. The Ti $2p_{3/2}$ and Ti $2p_{1/2}$ peaks are located at 458.7 and 464.4 eV, respectively, in agreement with the values for Ti^{4+} [26], indicating the ultrathin-film structure of TiO_2. In addition, the Pd 3d XPS data of SiO_2-Pd@30cyc-TiO_2 is consistent with that in Fig. S2b. It demonstrates that the chemical composition and valence state of Pd remain unchanged during the ALD growth of TiO_2. The STEM image, together with their energy-dispersive spectroscopy (EDS) mapping analyses (Fig. 1d–h), further proves the distribution of each element in this hybrid structure. Despite the relatively low contrast of STEM image, the EDS mapping clearly shows that the TiO_2 ultrathin film is evenly distributed on the surface of Pd nanocubes.

The thickness of TiO_2 ultrathin films can be readily tailored by varying the number of cycles during the ALD growth process. By reducing the number of growth cycles from 30 to 20, 10 and 5, the TiO_2 ultrathin films can be gradually shrunk down (Fig. 2). We name this series of hybrid structures as SiO_2-Pd@20cyc-TiO_2, SiO_2-Pd@10cyc-TiO_2 and SiO_2-Pd@5cyc-TiO_2 according to the cycles of ALD process. To assess the effect of TiO_2 film thickness on

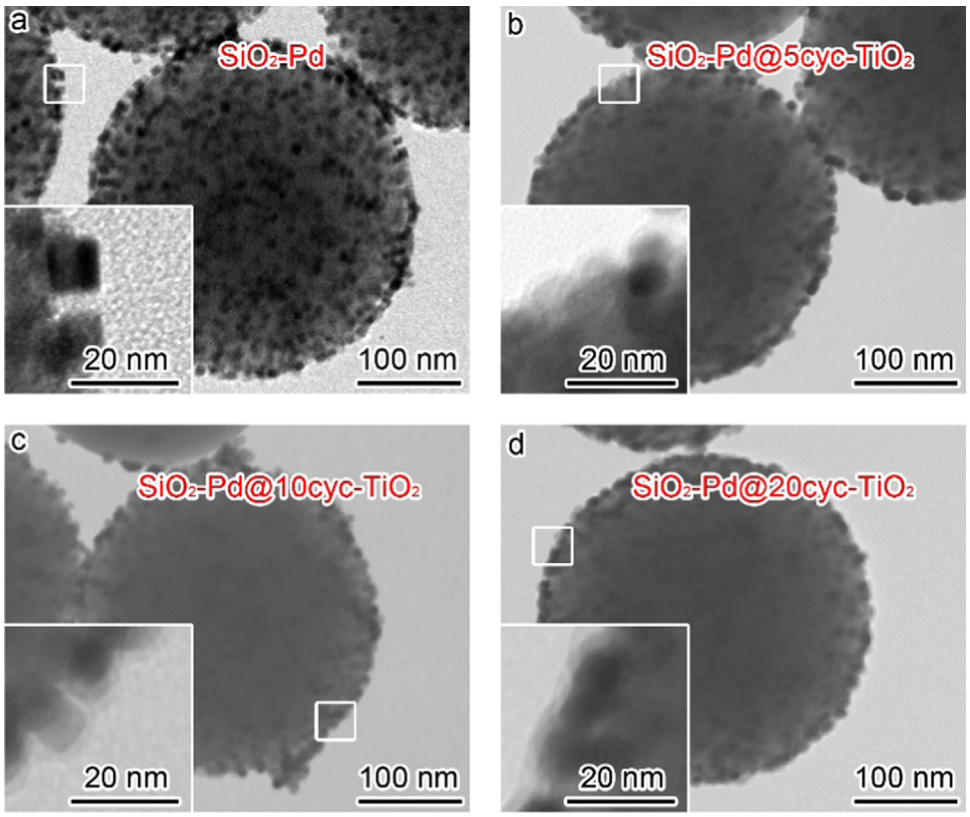

Fig. 2. TEM images of (a) SiO_2-Pd, (b) SiO_2-Pd@5cyc-TiO_2, (c) SiO_2-Pd@10cyc-TiO_2, and (d) SiO_2-Pd@20cyc-TiO_2. The insets show the magnified TEM images taken from the corresponding regions.

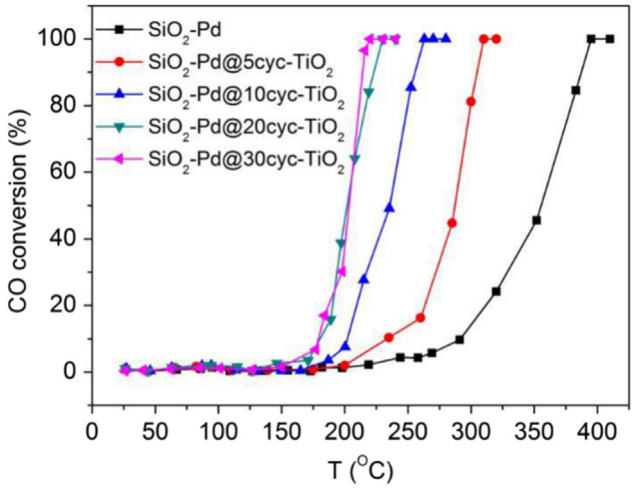

Fig. 3. Catalytic performance of SiO_2-Pd@5cycTiO_2, SiO_2-Pd@10cycTiO_2, SiO_2-Pd@20cycTiO_2 and SiO_2-Pd@30cycTiO_2 as compared with SiO_2-Pd hybrid structure in the oxidation of CO.

the catalytic performance of Pd, we maintain the same quantity of Pd in all the samples for CO oxidation. Meanwhile, we use SiO_2-Pd nanocubes as a reference sample to evaluate the impact of TiO_2 on Pd catalytic activity.

Fig. 3 shows the catalytic behaviors of SiO_2-Pd@TiO_2 and SiO_2-Pd samples for CO oxidation. The CO conv ersion rates turn out to increase in the order of SiO_2-Pd < SiO_2-Pd@5cyc-TiO_2 < SiO_2-Pd@10cyc-TiO_2 < SiO_2-Pd@20cyc-TiO_2 at nearly all reaction temperatures. This finding suggests that the increase of TiO_2 thickness can effectively promote the CO oxidation. Notably, we also recognize that the SiO_2-Pd@TiO_2 samples at 20 and 30 cycles exhibit very comparable catalytic performance.

To explore whether the parameter of 20 ALD cycles is the extreme borderline for catalytic performance enhancement, we intend to increase the thickness of TiO_2 coating by adding more ALD cycles (namely, SiO_2-Pd@40cyc-TiO_2, SiO_2-Pd@60cyc-TiO_2, SiO_2-Pd@80cyc-TiO_2, and SiO_2-Pd@100cyc-TiO_2). As revealed by Fig. 4, apparently the TiO_2 films can be thickened by increasing the growth cycles of TiO_2. Interestingly, all these samples nearly show the same catalytic activity in the CO oxidation (Fig. 5). This result proves that the TiO_2 with the thickness beyond 1.8 nm (i.e., the thickness of 20 cycles) cannot further boost the catalytic activity of Pd in CO oxidation.

The information gleaned above has revealed that the thickness of TiO_2 coated on Pd nanocubes has a great influence on the catalytic activity of Pd in CO oxidation. Upon establishing this relationship, we are now in a position to elucidate the mechanisms behind. In the case of SiO_2-Pd@TiO_2 hybrid structures, charge transfer occurs at the Pd-TiO_2 interface. The electrons are transferred from TiO_2 to Pd surface across their interface, as TiO_2 has a lower work function than Pd (4.1 eV versus 5.1 eV). As a result, the Pd surface near the interface possesses an increased electron density. As the amorphous TiO_2 formed via ALD is a porous film, the reactant CO and O_2 will access the Pd surface near the Pd-TiO_2 interface. At a high electron density, the Pd surface will offer more electrons to enter the antibonding orbital of CO and thus weaken the bonding of CO on Pd surface [9,27]. On the other hand, the high electron density will enhance the adsorption and activation of O_2 molecules on the catalyst surface [3,28]. Taken together, the limitation of Pd in CO oxidation can be overcome by increasing the electron density. As a matter of fact, the integration of Pd nanocubes with commercial TiO_2 (i.e., P25) can also improve the

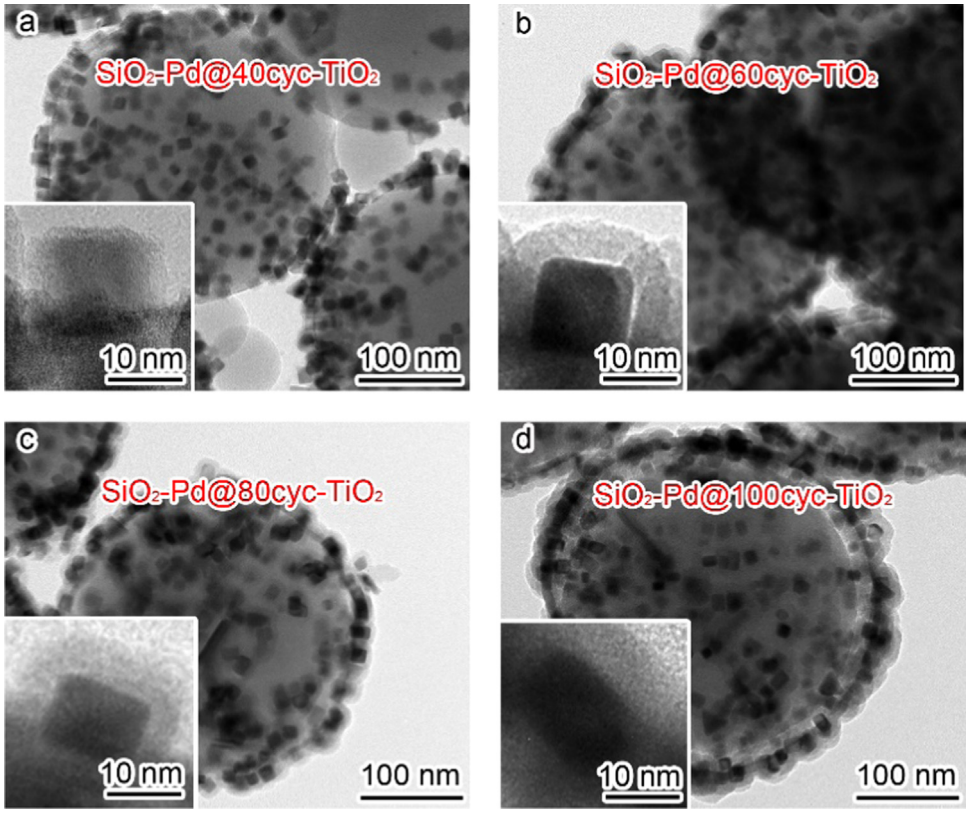

Fig. 4. TEM images of (a) SiO_2-Pd@40cyc-TiO_2, (b) SiO_2-Pd@60cyc-TiO_2, (c) SiO_2-Pd@80cyc-TiO_2, and (d) SiO_2-Pd@100cyc-TiO_2. The insets show the magnified TEM images taken from the corresponding regions.

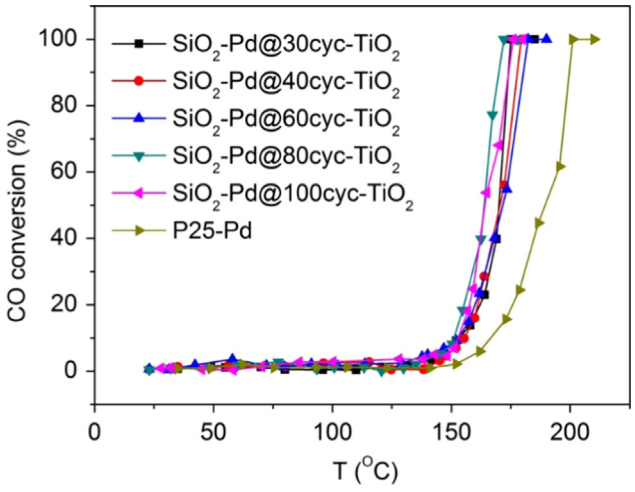

Fig. 5. Catalytic performance of SiO_2-Pd@40cycTiO_2, SiO_2-Pd@60cycTiO_2, SiO_2-Pd@80cycTiO_2 and SiO_2-Pd@100cycTiO_2 as compared with P25-Pd hybrid structure in the oxidation of CO.

catalytic CO oxidation as compared with bare Pd nanocubes (see the comparison of Fig. 5 with Fig. 3).

By increasing the ALD cycles from 5 to 20, thicker TiO_2 films should be capable of providing more electrons for Pd surface. As a result, the catalytic performance of Pd in CO oxidation has been gradually enhanced. Certainly this charge transfer effect, which is also called "polarization effect" in certain cases of catalysis, is limited by distance. With the continued increase of TiO_2 thickness beyond 1.8 nm, it would not bring more electrons to Pd surface for further enhanced CO oxidation as only the TiO_2 material within the distance can contribute to electron density tuning. For this reason, we only need to deposit a trace amount of TiO_2 onto Pd surface for the maximal CO oxidation activity using 20 ALD cycles. Another possible contribution from TiO_2 ALD film is the formation of interface-confined sites at Pd-TiO_2, at which the two oxygen atoms of an O_2 molecule can bind to both Pd and TiO_2 for enhanced adsorption and activation [29]. The porous nature of ALD TiO_2 allows forming these unique sites around the entire Pd cube surface, more abundant than that of the P25-Pd hybrid structure, where these sites only form near the bottom of the Pd cubes. As a result, the SiO_2-Pd@20cyc-TiO_2 sample exhibits dramatically higher activity than the P25-Pd hybrid structure (see Fig. 5).

4. Conclusions

In conclusion, we have developed an approach to coat amorphous TiO_2 ultrathin films on Pd nanocubes with precisely controllable thickness. The porous nature of ALD TiO_2 films allows reactant CO and O_2 molecules to access Pd surface for CO oxidation, as well as forms interface-confined Pd-TiO_2 sites for enhanced adsorption and activation. The intimate contact of TiO_2 with Pd can substantially increase the electron density of Pd surface, which depends on the TiO_2 thickness within 1.8 nm. The increased electron density can effectively overcome the limitation of Pd in CO oxidation – surface CO poisoning. As a result, by depositing a trace amount of TiO_2 as low as 20 ALD cycles (i.e., 1.8 nm), the catalytic performance in CO oxidation can be dramatically enhanced. This work opens up a new strategy for the rational design of hybrid nanostructures toward efficient catalytic reactions, and provides a new perspective for improving catalytic performance by regulating surface charge densities.

Acknowledgements

This work was financially supported by the NSFC (No. 21471141, 51402283), the Specialized Research Fund for the Doctoral Program of Higher Education (No. 20123402110050), the Recruitment Program of Global Experts, the CAS Hundred Talent Program, the Hefei Science Center CAS (2015HSC-UP009), and the Fundamental Research Funds for the Central Universities (No. WK2060190025, WK2310000035, WK2060030014 and WK2060190026).

Appendix A. Supplementary material

Supplementary data associated with this article can be found in the online version at http://dx.doi.org/10.1016/j.pnsc.2016.05.010.

References

[1] Y. Bai, W. Zhang, Z. Zhang, J. Zhou, X. Wang, C. Wang, W. Huang, J. Jiang, Y. Xiong, J. Am. Chem. Soc. 136 (2014) 14650–14653.
[2] W.N. Wang, W.J. An, B. Ramalingam, S. Mukherjee, D.M. Niedzwiedzki, S. Gangopadhyay, P. Biswas, J. Am. Chem. Soc. 134 (2012) 11276–11281.
[3] R. Long, K. Mao, M. Gong, S. Zhou, J. Hu, M. Zhi, Y. You, S. Bai, J. Jiang, Q. Zhang, X. Wu, Y. Xiong, Angew. Chem. Int. Ed. 53 (2014) 3205–3209.
[4] H.J. Freund, G. Meijer, M. Scheffler, R. Schlögl, M. Wolf, Angew. Chem., Int. Ed. 50 (2011) 10064–10094.
[5] X.Y. Deng, B.K. Min, A. Guloy, C.M. Friend, J. Am. Chem. Soc. 127 (2005) 9267–9270.
[6] Y.H. Zhang, X.F. Weng, H. Li, H.B. Li, M.M. Wei, J.P. Xiao, Z. Liu, M.S. Chen, Q. Fu, X.H. Bao, Nano Lett. 15 (2015) 3616–3623.
[7] X.W. Yu, P.G. Pickup, Electrochem. Commun. 11 (2009) 2012–2014.
[8] S. Bai, C. Wang, M. Deng, M. Gong, Y. Bai, J. Jiang, Y. Xiong, Angew. Chem. Int. Ed. 53 (2014) 12120–12124.
[9] S. Bai, L. Yang, C. Wang, Y. Lin, J. Lu, J. Jiang, Y. Xiong, Angew. Chem. Int. Ed. 54 (2015) 14810–14814.
[10] A.L. Linsebigler, G.Q. Lu, J.T. Yates, Chem. Rev. 95 (1995) 735–758.
[11] Y. Sun, S. Gao, Y. Xie, Chem. Soc. Rev. 43 (2014) 530–546.
[12] A. Hellman, S. Klacar, H. Grönbeck, J. Am. Chem. Soc. 131 (2009) 16636–16637.
[13] Y. Sun, F. Lei, S. Gao, B. Pan, J. Zhou, Y. Xie, Angew. Chem. Int. Ed. 52 (2013) 10569–10572.
[14] Y. Sun, Q. Liu, S. Gao, H. Cheng, F. Lei, Z. Sun, Y. Jiang, H. Su, S. Wei, Y. Xie, Nat. Commun. 4 (2013) 2899–2906.
[15] D. Hausmann, J. Becker, S.L. Wang, R.G. Gordon, Science 298 (2002) 402–406.
[16] S.M. George, Chem. Rev. 110 (2010) 111–131.
[17] J. Lu, J.W. Elam, P.C. Stair, Acc. Chem. Res. 46 (2013) 1806–1815.
[18] J. Aarik, A. Aidla, T. Uustare, M. Ritala, M. Leskelä, Appl. Surf. Sci. 161 (2000) 385–395.
[19] T.W. Hamann, A.B.F. Martinson, J.W. Elam, M.J. Pellin, J.T. Hupp, J. Phys. Chem. C 112 (2008) 10303–10307.
[20] F. Hao, J. Lu, P. Stair, J.W. Elam, Catal. Lett. 141 (2011) 512–517.
[21] X. Xie, Y. Li, Z. Liu, M. Haruta, W. Shen, Nature 458 (2009) 746–749.
[22] W.C. Huang, L.M. Lyu, Y.C. Yang, M.H. Huang, J. Am. Chem. Soc. 134 (2012) 1261–1267.
[23] L. Wang, J. Ge, A. Wang, M. Deng, X. Wang, S. Bai, R. Li, J. Jiang, Q. Zhang, Y. Luo, Y. Xiong, Angew. Chem. Int. Ed. 53 (2014) 5107–5111.
[24] A. Imanishi, E. Tsuji, Y. Nakato, J. Phys. Chem. C 111 (2007) 2128–2132.
[25] W. Stöber, A. Fink, J. Colloid Interface Sci. 26 (1968) 62–69.
[26] D. Briggs, M.P. Seah, Practical Surface Analysis, vol. 1, John Wiley & Sons, New York, 1993.
[27] F.A. Cotton, G. Wilkinson, C.A. Murillo, M. Bochmann, Advanced Inorganic Chemistry, Wiley, USA, 1999 6th ed..
[28] Z. Zhang, J.T. Yates, J. Am. Chem. Soc. 132 (2010) 12804–12807.
[29] Q. Fu, W.X. Li, Y. Yao, H. Liu, H.Y. Su, D. Ma, X.K. Gu, L. Chen, Z. Wang, H. Zhang, B. Wang, X. Bao, Science 328 (2010) 1141–1144.